

RADAR MAPPINGS FOR ATTITUDE ANALYSIS OF OBJECTS IN ORBIT

S. Lemmens⁽¹⁾, H. Krag⁽¹⁾, J. Rosebrock⁽²⁾, and I. Carnelli⁽³⁾

⁽¹⁾European Space Agency, ESOC/HSO-GR, 64293 Darmstadt, Germany. Email: stijn.lemmens@esa.int

⁽²⁾Fraunhofer Institute for High Frequency Physics and Radar Techniques, FHR, 53343 Wachtberg, Germany

⁽³⁾European Space Agency, HQ/PPC-PF, 75738 Paris, France

ABSTRACT

Inverse synthetic aperture radars (ISAR) are a valuable instrument for assessing the dynamic state of a large object in low Earth orbit. In particular, the images generated by these radars can reach a sufficient resolution to be used during launch support or contingency operations in low Earth orbit, i.e. for confirming the deployment of structures, determining the structural integrity, or analysing the dynamical behaviour of an object. However, the direct interpretation of ISAR images can be a difficult task due to the nature of the range-Doppler space in which these images are produced. To support the interpretation process, a tool has been developed by ESA's Space Debris Office to generate radar mappings of a target in orbit. Such mappings are a 3D-model based simulation of how an ideal ISAR image would be generated by a ground based radar under given processing conditions. As the process for generating ISAR images assumes a scattering body, a rudimentary 3D model of the target is sufficient in order to derive information from the generated maps. Processing predefined attitude states in comparison with actual observations allows it to detect non-nominal behaviour or to determine attitude states of the target.

Key words: ISAR images, radar mappings, attitude determination.

1. INTRODUCTION

In almost 50 years of space activities more than 4800 launches have placed more than 5000 satellites in orbit, of which only a minor fraction of about 1000 are still operational today. Besides this large amount of intact space hardware, with a total mass of about 6000 tonnes, several additional objects are known to orbit the Earth. They are regularly tracked by the US Space Surveillance Network and, today, more than 16000 of them are maintained in their public catalogue, which covers objects larger than approximately 5cm to 10cm in low Earth orbit (LEO) and 30cm to 1m at geostationary altitudes (GEO). Only 6% of the catalogued orbit population are operational spacecraft, while 28% can be attributed to decom-

missioned satellites, spent upper stages, and mission related objects (launch adapters, lens covers, etc.). The remainder of about 66% is originating from more than 200 on-orbit fragmentations which have been recorded since 1961. The high impact velocities, which can reach 15km/s for most missions in LEO, are the reason for the destructive energy, even despite of the small object sizes. So far, there are four recorded examples of collisions, with the latest and most prominent one between the active Iridium-33 satellite and the decommissioned Cosmos-2251 satellite.

Today, there is little knowledge on the attitude state of decommissioned objects. Observational means have advanced in the past years, but are still limited w.r.t. accurately estimating the orientation of the motion vector and its magnitude or objects. In general, the attitude evolution of a decommissioned object is expected to be irregular at first, and regularise slowly under the influence of external torques. The actual attitude evolution depends strongly on the inertia tensor of the object and is influenced by the environment. E.g. gravity will induce a torque on elongated bodies as will a mismatch between the barycentre of the projected surface in flight direction. Moreover, internal components like reaction wheels and gyros or rotating disks might transfer momentum to the satellite body. Observations in the past, e.g. by the Fraunhofer Institute for High Frequency Physics and Radar Techniques (FHR) Tracking and Imaging Radar (TIRA) applying ISAR techniques, have mainly concentrated on objects which were about to undergo an uncontrolled re-entry in the following days. In a few cases attitude rates of about 10 deg/s have been estimated in this way. Generation of so-called light curves, i.e. evolution of the brightness of space objects in the visible region, with the help of optical telescopes is a second promising measure to estimate attitude rates of targets in higher altitudes. Furthermore, laser ranging could be a promising means to identify varying offset of a reflective surface from the centre of mass of the parent body. In all cases, research is required to further improve the resolution of the data and/or to fit geometric models into the measurements for an estimation of the attitude.

In this paper, we will focus on the software required to interpret and simulate ideal ISAR images with as goal the determination of the attitude evolution of an object in

orbit. To this end, a new software library has been developed with the focus on so called radar mappings. Such mappings are a 3D-model based simulation of how an ideal ISAR image would be generated by a ground based radar under given processing conditions. This technology is a valuable tool for spacecraft operators for the analysis of their spacecraft, e.g. during a contingency, where the identification of the attitude motion is key element in the process, or to confirm the deployment of structures. Moreover, knowledge on the rotational state, and its predictability, of an object is a driver for the preparation of an active debris removal mission. For example, attitude motions above a few degree per second will impede to use classical robotic capture mechanisms. In Section 2, the nature of the ISAR imaging plane which we want to reconstruct is described. In Section 3, a high level description of the developed software library is given, which is then used in practice for determining the attitude of one passage of ESA's Envisat satellite in Section 4.

2. GEOMETRIC PROPERTIES OF ISAR IMAGING

Inverse synthetic aperture radar (ISAR) is the denomination for a technique where a fixed system is collecting data from a moving target, and by analysing the Doppler histories of scattering centres creates a synthetic aperture. For the mathematical background of this process, the reader is referred to [3]. In this section, we will focus on the generation and orientation of the image plane associated to this technique when applied to objects in space.

In ISAR imaging, the image plane lies quite different from the optical one. The line of sight (LOS) is embedded in the image plane and not orthogonal to it as in optics. The other dimension of the image plane depends on the rotational motion of the object. In general, the set of LOS vectors at different times in the object-fixed coordinate system spans a surface. Usually, this surface can be approximated by a plane which can then be identified as the image plane. This is especially the case for comparatively small angles between the LOS vectors at different times, corresponding to a small time interval.

The ISAR image then is the sum of the parallel projections to the image plane of the set of all scatterers of the object, weighted by their amplitudes and convolved by the point scatterer response of the system. In certain observation situations, the surface spanned by the LOS vectors is exactly a plane, if Earth rotation is ignored. One such case is, for example, a zenith pass of a satellite in which the orbit vector, from Earth centre to the satellite, is fixed and is not rotating around an axis in the orbit plane. Another example is an object on a straight path relative to the Earth coordinate frame and not rotating in this frame. If the attitude of the satellite is always known, the surface spanned by the LOS vectors is also known and the image plane can be determined from that knowledge. However, in general Earth rotation has to be taken into

account.

Another way to conceive the rotational motion of a satellite is to divide its rotation into two components: One component is the rotation of a coordinate system with one axis tied to the LOS vectors relative to an assumed stabilised attitude of the satellite. The second component, called intrinsic rotation, is the rotation of the assumed stabilised satellite relative to the real satellite attitude. The intrinsic rotation is usually not known and difficult to determine. Therefore, in the imaging process it is often assumed to vanish. The composition of both rotational motions yields the rotation of the coordinate system with one axis tied to the LOS vectors relative to the real satellite attitude as required. Conversely, this establishes a so called turntable situation, in which the satellite rotates relative to the coordinate system tied to the LOS and in which the range variation of each scatterer is sinusoidal with a frequency proportional to the rotational velocity.

3. SOFTWARE SUITE

In order to facilitate generating radar mappings to simulate an idealised ISAR image, all standard routines from astrodynamics and rotational kinematics are required. Moreover, a novel algorithm to compute the radar mapping from a 3D-model had to be developed as, to the best of our knowledge, no open software library offered this capability. Therefore, it was decided to implement all necessary routines in a self-contained library which would serve as base for further applications. Python was used for the implementation because of its modularity, interpreters allowing rapid development of applications, plotting tools and interfacing capabilities with compiled languages. When speed is required for an algorithm and the input is rigid, e.g. orbit or attitude propagation, the implementation is done in Fortran, called by the Python library at runtime.

3.1. General functionality

The Models on Orbit With an Attitude (MOWA) library is build up in three layers. The first layer contains the general functionalities, implemented following the procedural programming paradigm, for dealing with coordinate and time transformations, Input/Output and error handling routines, and low level support functions. The second layer, building on top of the first one, contains the core computational functionalities, implemented following the object oriented programming paradigm. It features modules for dealing with state vectors, attitude states, observations, Earth parameters and physical constants, propagators for orbit and attitude states, and the modelling of three dimensional objects. The third layer provides modules for dealing with objects from the second layer in a unified manner, again following the object oriented programming paradigm. The functionalities include grouping state vectors and attitude states into full

ephemerides, and, if required, combining them with an 3D object model, allowing to simulate observations or vice versa. A module is added for straightforward visualisation of the ephemeris and observation data for quick inspections.

As with all Python based libraries, the functionalities of all levels are available to the users, enabling them to write programs beyond the capabilities already provided by the third layer of MOWA. For example, a script was developed which takes as input the model of an upper stage, or more general any payload or rocket body, and allows the user to compute the average geometrical cross-section along the orbit for different attitude scenarios. A more elaborate example of these extension capabilities is described in Section 4, where the goal is to fit attitude states to ISAR images of a target.

3.2. Three dimensional modelling and observation simulation

One of the *raison d'être* of MOWA was to enable the fitting of simulated observations to actually observed images, both optical and ISAR in nature. Therefore, a module was added to simulate images from predefined models as they would be perceived by a telescope as well as by an imaging radar installation. For the ISAR images, we do not simulate the entire process of transforming Doppler-Range measurements of a scattering body into an image. Rather, we simulate how an ideal ISAR image would look like when the model is geometrically known, and only the attitude state of the object and the geometry between observer and observable are taken into account. We thus speak about *radar mappings* rather than simulating ISAR imaging in this context.

Objects can be geometrically modelled in MOWA by specifying the vertices, facets and normals as respectively points, triangles and vectors in three dimensional Euclidean space. Vertices define the facets which define a mesh, which is in turn interpreted as the 3D-model. The data is stored as plain text and the structure follows closely the OBJ and MTL file format specifications, first developed by Wavefront Technologies, for representing 3D geometries. This makes the model human readable and allows exporting toward and importing from other 3D modelling software compatible with the OBJ format. As extensions to the OBJ specifications, the model can be optionally used to store cross-section information and moments of inertia. Parts of the MTL specifications are implemented to store basic surface information, e.g. diffuse and specular reflectivity for different wavelengths, on the materials used for the model's facets.

Many open libraries offer the possibility to generate normal, optical, images from arbitrary view points. However, such an option does not exist for the generation of ISAR images, and would require some work to implement in most popular imaging libraries. As a consequence, it was decided that, at least for initial development purposes, a radar mapping algorithm would be

implemented from scratch. To generate optical images, the algorithm loops over all facets of the model and computes the boundaries of the triangles in three dimensional Cartesian coordinates. These boundaries are converted from the model coordinate system to a user defined camera coordinate system, by orthogonally projecting them into the image plane of the camera, and a z-buffer of the projected points is stored to resolve the visibility of facets. The boundaries of the triangles in the image plane are drawn by Bresenham's line algorithm [1] and coloured. To generate a radar mapping of a model, we start the same way as for an optical image, but we define a second image plane by using the direction of the orthogonal projection as image y-axis and keeping the x-axis as for the optical image. The values of the z-buffer are augmented with an identifier to keep track of which facet generated the lowest z-buffer value. The distance values of the z-buffer are marked in the new image plane with their corresponding x-axis value, which generates the mapping. We note that it is often the case that two distinct points on the model contribute to the same pixel in the radar mapping. The user can define different output behaviours of this superposition, e.g. taking into account the reflectivity properties of the materials as defined by the MTL specifications.

3.3. Fitting radar mappings to actual observations

The direct interpretation of ISAR images is hampered due to the fact that they are generated based on the theory of scattering, which can lead to distorted images and a reduction in feature resolution scale. Moreover, to an average human the range-Doppler plane in which these images are displayed is a non-intuitive geometrical environment and requires some a priori assumptions on the rotational state of the target. This in turn means that it is hard to transform well studied computer vision concepts, such as structure from motion or feature tracking, to a radar setting when working with a non-trivial 3D-model. These concepts have been studied in [8, 5, 4, 6]. Before embarking along those paths of investigation, it was decided to implement routines for forward modelling, i.e. generating the radar mapping from a model and fitting the attitude by comparing the mappings to the observations.

The nature of ISAR images, with examples given in Figures 5 (left) and 7 (left), impedes their direct usage for a fitting process. The colours in the ISAR images are pseudo-colours indicating the strength of the reflected radar waves by the scatterers on the object. First, they are pre-processed to extract the shape of the object under scrutiny into a binary, e.g. black and white, image, either by a human interpreter or computer algorithm. Some parts of the object reflect the radar waves only moderately, or display a certain regularity, which makes it easy for a human interpreter to find the edges of a shape. An example of this is the solar panel left in Figure 5 (left). On the other hand, many scattering objects closely together make it hard to establish a clear boundary and to relate it back to its basic shape, as can be seen in both Figures 5

(left) and 7 (left). Moreover, highly reflective parts can generate smeared-out streaks in the image, e.g. the ones from the high gain antenna in Figure 7 (left). In most cases, a human interpreter outperforms a classical edge detection based algorithm when making educated guesses concerning the underlying shape defining the ISAR image. To provide an initial, conservative, shape extraction which can be further fine-tuned by a human interpreter, the following algorithm is applied to an ISAR image:

1. A low pass filter is applied to remove the dark background and leave most of the highly reflective parts visible.
2. An opening operator, i.e. dilation of the erosion [7], is ran over the image to remove the remaining noise from the foreground.
3. A closing operator, i.e. erosion of the dilation [7], is ran over the image to turn small background patches into foreground.
4. A Gaussian filter is applied to the image, to assure that parts likely to be connected in reality are connected in the image.
5. All colour is removed to form a binary image.

The procedure above, generally overestimates the size but provides a good initial guess. The results from applying this algorithm to the radar observations in Figures 5 (left) and 7 (left), are given in Figures 5 (right) and 7 (right), respectively. They can be compared to the variants generated by a human interpreter, given in respectively Figures 5 (middle) and 7 (middle).

Once a shape has been extracted and stored as a binary image, it can be used as a reference for the radar mappings when determining a best fit. The parameter to be fitted is the attitude of the model in an inertial frame, in order to generate the most similar shape when mapped. To this extent, two algorithms have been developed. The first one is a brute-force strategy, allowing the user to search within a predefined attitude window to the best match, either in a structured or random way. The second one is a gradient-descent optimiser which allows searching through attitude space with variable step-size from a given initial attitude. The gradient is computed numerically for a given cost function. The brute-force strategy is a valid starting point when a first attitude has to be found for a given sequence. Whereas the gradient-descent strategy provides good results when an attitude for one step in a sequence is known and the next one has to be fitted.

Both search strategies require a cost function to determine the quality of a fit. The default cost function is determined from the areas of the reference shape and the generated radar mapping. First, the percentage of the area of the reference shape not overlapped by the radar mapping w.r.t. reference shape area is computed. Secondly, the percentage of the radar mapping not overlapping the reference shape w.r.t. the area of the radar mapping is

computed. Both values are required to avoid yielding a small value of the cost function when presented with a skewed ISAR images or radar mappings. To get the overall cost function, both values are combined linearly with user defined weights.

The accuracy of this fitting process is estimated, by varying the attitude of an optimal fit, to be in the order of degrees when described with Euler angles. Dedicated radar observations of a target with a precisely known attitude state would provide the ideal opportunity to further test the accuracy of the fitting method. This accuracy reflects on the process of deriving results from a fitted sequence of observations. For example, the user can define custom coordinate systems on the 3D-model, e.g. intended to simulate a particular sensor. The incidence of the directional vector, e.g. towards a point on the Earth of the Sun, on these sensor coordinate systems can be computed for the fitted sequence. This can help to determine the likelihood of various scenarios, e.g. communication with an Earth station or power generation with solar cells.

4. ASSESSING THE ATTITUDE OF ENVISAT AFTER THE FINAL ANOMALY

After 10 years of service, ESA's Earth observing satellite Envisat stopped sending data to ground from 8 April 2012 onwards. Following rigorous attempts to re-establish contact and the investigation of failure scenarios, the mission was declared over on 9 May 2012. The satellite is therefore stranded in Sun-synchronous orbit at an altitude of around 760 km. The ISAR images made from Envisat after the final anomaly, of which two are displayed in this paper, are obtained by the space observation radar TIRA, operated by the Fraunhofer Institute for High Frequency Physics and Radar Techniques. The radar primarily serves as the central experimental facility for the development and investigation of radar techniques for the detection and reconnaissance of objects in space. TIRA offers space agencies the possibility to measure the orbit of objects with high precision or produce a high resolution image of objects such as satellites.

In the following paragraphs, the results of using the MOWA library to study the attitude of Envisat as observed by TIRA during the passage of 2012-05-23, rising above the horizon at 11:44, are presented. Given the resolution of the ISAR images at hand, the model used for fitting radar mappings does not have to be detailed. It is however important to have the overall dimensions of the scattering elements correct if we want to compute an accurate attitude. In the case of Envisat, the important parts to model, i.e. driving the overall appearance for the ISAR image, are therefore:

- The main body, represented as a box.
- The Advanced Synthetic Aperture Radar (ASAR) antenna, represented as a flat plate without worrying about its inclination w.r.t. the main body.

- The solar panel, front and back side as they were found to reflect differently in the ISAR image due to the nature of the materials, represented as thin plates with a empty separation between them.
- The radar-reflecting high gain antenna, represented as a spheroid dish.
- The connections between all the parts.

From previous ISAR imaging passages, it was deduced that the solar panel was not rotating and fixed in an anti-canonical position, i.e. opposite to what was expected in a safe mode. This conjecture was confirmed by the acquisition of optical observation, reproduced in Figure 1, by the French Earth observing satellite Pleiades 1, and therefore reflected in the 3D-model. The front and back side are coloured differently in the radar mappings and in the generated optical observations for convenient verification by a human interpreter, but otherwise the distinction was not used by the fitting algorithm. The model is visible in two different orientations in Figures 6 (right) and 8 (right).

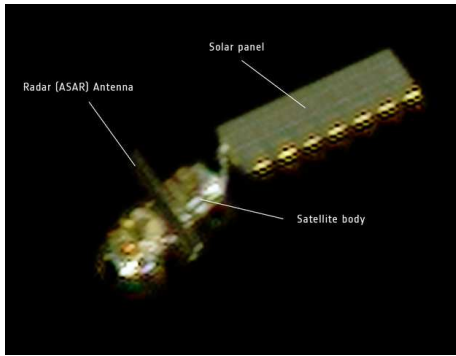


Figure 1: Pleiades image of Envisat (CNES)

4.1. Radar mapping during the passage of 2012-05-23 11:44

When presented with a set of ISAR images of a target from a given sensor location, one is generally interested in knowing the attitude of the target with respect to a pre-defined coordinate system in space, on Earth, or along its orbit. Irrespective of the desired coordinate system of comparison, the attitude in an inertial system has to be computed before it can be transformed. Therefore, the orbit of the target at the times of the ISAR image generation has to be known. The MOWA library allows for the direct computing of the orbit at these points, by means of propagating an initial state, and transform all required states into an inertial reference system.

The Doppler shift which is used to generate an ISAR image comes from the change in aspect angle. For a stabilised motion, the Doppler axis, also called the cross axis, of the image plane is therefore determined by the

unit vector computed from the subtraction of the LOS vector relative to a target-fixed coordinate system from one observation from the previous one. The rotation axis is thus perpendicular to the plane determined by the two LOS vectors. Here we assume an inertial stabilisation, i.e. that the target doesn't rotate in the inertial system. If the image scaling orthogonal to the LOS in the ISAR images generated due to the assumption of vanishing intrinsic rotation is obviously wrong, an additional intrinsic rotation can be guessed as described in Section 2. Then the Doppler axis vector is the sum of two components. The first component is the direction determined by the LOS vectors relative to the stabilised, i.e. inertial, system, as in the previous case. The second component lies within the assumed plane of the intrinsic rotation and is proportional to the assumed intrinsic rotation velocity. In our case, the intrinsic rotation plane is assumed to coincide with the orbit plane. The second component thus lies in the orbit plane. Only in the case of a zenith pass will it always lie in the image plane as well.

In the case of this observation sequence, an intrinsic rotation of $0.2^\circ/s$, with axis perpendicular to the orbit plane, had to be assumed to scale the ISAR image. This is already a clear indication that Envisat was not in its default Earth observing attitude, which would otherwise yield an intrinsic rotation of $\sim 0.06^\circ/s$ with its axis of rotation perpendicular to the orbit plane.

The image plane for the radar mapping is then defined by using the normalised LOS as y-axis and the normalised Doppler axis as x-axis. By assuming an inertial reference system, these axes have an interpretation in the 3D model reference frame. In the latter frame, we define the body fixed axes to coincide with the coordinate axes for the default attitude, i.e. the unit quaternion. The difference in computation of the image axes between the original observations and the radar mappings is shown in Figure 2. The small offset in image axes can be explained by the use of slightly different state vectors and is within the estimated accuracy of the fitting method.

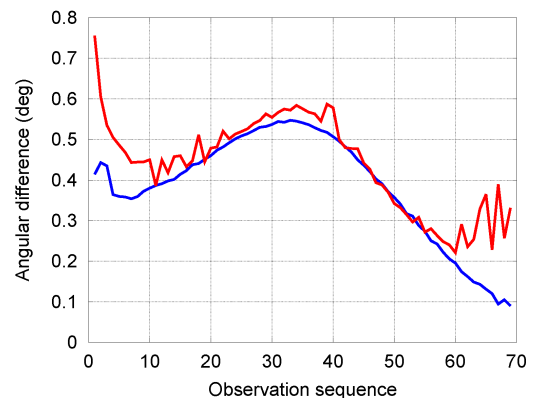


Figure 2: The difference in computing radar mapping image axes, where the blue curve corresponds to the range vector and red to the Doppler, i.e. cross, vector, between TIRA and MOWA.

Table 1: Selected output of attitude states for the passage of Envisat on 2012-05-23 11:44 as observed from TIRA and described as rotations, in Euler angles, of the model w.r.t. the RTN coordinate system. See Appendix A for the conventions applied when using Euler angles.

Epoch hh:mm:ss.ms (UTC)	Phi (deg)	Theta (deg)	Psi (deg)
11:48:51.2128	17.5	40.6	43
11:49:00.2128	24.2	43.0	42.9
11:49:09.2128	28.3	43.5	43.3
11:49:18.2128	33.6	45.5	43.2
11:49:27.2128	35.6	46.4	43.0
11:49:36.2128	40.5	48.4	43.3
11:49:45.2128	40.7	48.9	54.4
11:49:54.2128	41.9	49.8	58.9
11:50:03.2128	48.5	47.1	59.9
11:50:12.2128	49.8	48.5	65.9

The MOWA library allows to store orbital state vectors as well as attitude states. The radar mapping can be directly compared to the observational image to check if the predefined attitude is plausible. A GUI is being developed which enables an operator to quickly study different attitude scenarios, e.g. default operations mode or safe mode, by generating the radar mappings for different scenarios and comparing them to the actual observations.

4.2. Fitting attitude results

For the fitting of radar mapping to the passage on 2012-05-23 11:44, MOWA was configured to return a radar mapping, an accompanying optical observation and the associated cost function metric for every attitude it processed. On average, with RGB colour scale images on pixel resolution of 600x600, 100 attitude states could be processed, with results returned in 57 seconds on a single Intel Xeon CPU, X5660, at 2,80GHz. Given the nature of the task, this leaves room for parallelising the computations depending on the search strategy. The optimal fitted radar mapping yields the attitude states in either an inertial system or the Radial, Transverse, Normal (RTN) reference frame along the orbit. An example of the attitude history output is given in Table 1.

The best fit radar mappings for two selected points in the observation sequence are given in Figures 6 (left) and 8 (left), for respectively the observations in Figures 5 and 7. The radar mapping in Figure 8 with w.r.t. to the observation in Figure 7 demonstrates the ability of the algorithm to find an optimal solution, even when dealing with complex shading. Also the position of the high gain antenna is a close match and displayed correctly.

From the estimated attitude states in an inertial reference frame, we can deduce the rotational motion of the 3D-model by converting the changes in attitude to rotations around axes defined in the body-centric, or 3D-model, coordinate system. This can be achieved by computing the

rotation matrix with the triad method [2], and transforming it to an Euler axis angle pair. Moreover, the obtained rotation axes can be interpreted in the original inertial, depending on the application. From the resulting angles, we get a feeling for the angular velocity of the 3D-model during the observations. In Figure 3, the estimated angular velocity in degree per second is shown for each of the observation steps. The five largest angular velocities correspond to observations where the fitting algorithm alone was insufficient to find the correct next attitude when starting from a previous one. The cause for these offsets will be further explained in Section 4.3. When excluding the five outliers from the series, the mean, median and standard deviation of the estimated angular velocity are respectively $0.83^\circ/s$, $0.75^\circ/s$ and $0.37^\circ/s$.

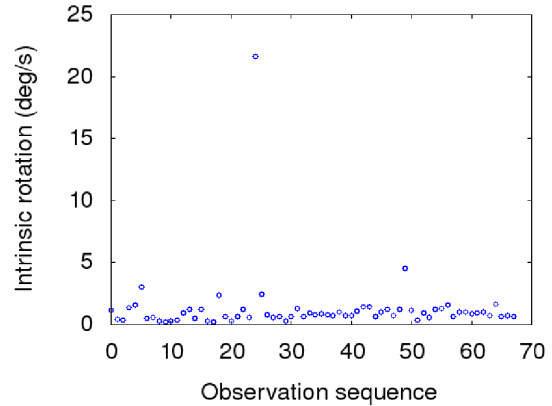


Figure 3: The estimated angular velocity of Envisat as computed from the simplified model, fitted via radar mappings to the observations of 2012-05-23.

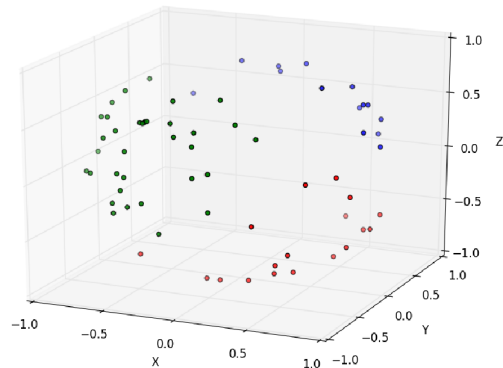


Figure 4: The orientation of the rotation axis of Envisat, in the body-centric, i.e. model's, coordinate system, as computed from the simplified model, fitted via radar mappings to the observations of 2012-05-23. The green (35), red (19) and blue (14) colours group orientations with similar direction as determined with a 3-means clustering algorithm.

In Figure 4, the locations of the rotation axis in the body-

centric frame are plotted on the unit sphere. This allows, in theory, to estimate effects such as precession and nutation when the inertia tensor of the object under study is accurately known. This is, however, not the case here and given that the estimated angular velocities are within the accuracy of the fitting procedure, we should be careful to draw conclusions from this data. In broad terms, the rotation axes can be confined to one half of the unit sphere and can be grouped together in three clusters. This hints at a well defined pattern in the attitude. However, fitting results over many passages have to be studied before this pattern can potentially be extracted. The clustering is established with a k-means algorithm. The separation between the blue and green group is due to the fitting algorithm and will be elaborated upon in Section 4.3. The red group are mostly spurious offsets of the green group, and sometimes from the blue group. They are conjectured to correspond to noise on the fitting procedure.

4.3. Solar panel offset

As alluded to in the previous section, the fitting algorithm was not always capable of finding a minimum in the cost function that would represent the correct physical attitude, requiring a human interpreter to interfere. Specifically on observations made when the solar panel's visibility switched from the front to the back side, or vice versa, it became clear that the assumption of an anti-canonical solar panel orientation for the 3D-model does not match the observations. However, as the shape of the main body as computed for the radar mapping can be fitted within the noise of the ISAR image, this mismatch is not visible in most of the observations. This can be understood by the fact that the algorithm focusses most on fitting the solar panel due to its large projected area. Thus when the projected area of the main body dominates, the algorithm yields a different intrinsic rotation axis for the fitted radar mappings. This effect can be seen in Figure 4, where the location of the 14 blue unit vectors all arose during the fitting of the first 27 observations, where the main body was the dominating factor in the area estimation. After the 27th observation, the algorithm had to be reset and focussed on the panel for determining the attitude. This corresponds with the large jump in angular velocity in Figure 3. Preliminary assessments indicated that the offset of the solar panel from an anti-canonical position can be accounted for up to 10° . A more detailed analysis will be performed to get the most accurate value based on some of the radar observations, and the observation sequence will be reprocessed to quantify how an offset in the model influences the fitting process.

5. CONCLUSIONS

In this paper, we reported on the development of the MOWA software library dedicated to support the interpretation of ISAR images. To this extent, the concept of radar mappings, i.e. the 3D-model based simulations

of how an ideal ISAR image would be generated, and functionalities to fit them to actual observation sequences have been implemented. Fitting radar mappings to observed ISAR images allows to reconstruct the attitude history of an object, and display the data in a frame relevant for an operator or an analyst. These techniques have been demonstrated on the case of ISAR imaging data acquired from ESA's Envisat satellite on 2012-05-23, for which we estimated an angular velocity of $0.85^\circ/s$ during the observation sequence. Moreover, with the help of the MOWA library, attitude scenarios can be defined based on the 3D-model geometry, e.g. the attitudes required for a Sun or Earth pointing sensor, and their simulated radar or optical observations computed. This enables the straightforward detection of unexpected behaviour, or confirm nominal behaviour such as the deployment of structures, when compared with actual observations.

ACKNOWLEDGEMENTS

The authors would like to thank Benjamin Bastida Virgili, Klaus Merz, Tim Flohrer, Heiner Klinkrad and Quirin Funke for many fruitful discussions during the development cycle of the software library. Furthermore, we would like to thank ESA's General Studies Programme for their support.

REFERENCES

1. Bresenham, J. E., (1965), *Algorithm for computer control of a digital plotter*, IBM Systems Journal, vol. 4, issue 1, pp. 25-30.
2. Black, H., (1964), *A Passive System for Determining the Attitude of a Satellite*, AIAA Journal, vol. 2, issue 7, pp. 1350-1351.
3. Borden, B. (1999), *Radar Imaging of Airborne Targets*, Institute of Physics Publishing, ed. 1.
4. Ferrara, M., Arnold, G., and Stuff, M. A., (2009), *Shape and Motion Reconstruction from 3D-to-1D Orthographically Projected Data via Object-Image Relations*, IEEE Transactions On Pattern Analysis and Machine Intelligence, vol. 31, no. 10, pp. 1906-1912.
5. Rosebrock, J., (2006), *3-D point scatterer estimation for 3-D ISAR imaging and attitude determination*, Proceedings of the 6th European Conference on Synthetic Aperture Radar.
6. Rosebrock, J., (2011), *Absolute Attitude From Monostatic Radar Measurements of Rotating Objects*, IEEE Transactions On Geoscience And Remote Sensing, vol. 49, no. 10, pp. 3737-3744.
7. Soille, P., (2004), *Morphological Image Analysis: Principles and Applications*, Springer, ed. 2.
8. Stuff, M. A., (2000), *Three dimensional Invariants of Moving Targets*, Algorithms for Synthetic Aperture Radar Imagery VII, Proceedings of SPIE, vol. 4053.

A. APPENDIX: IMAGES AND MAPPINGS

This appendix is dedicated to examples of ISAR images and radar mappings. We describe the circumstances for two distinct observations made by TIRA during the pass of Envisat and represent graphically the optimal radar mapping computed with the MOWA library as described in Section 4. The figures are presented in the following order:

1. The ISAR images as provided by Fraunhofer FHR.
2. The black and white reduction of the ISAR image to its core shape by a human interpreter.
3. The black and white reduction of the ISAR image to its core shape by a computer algorithm.
4. The best fit radar mapping for the given model.
5. The simulated optical observation of the best fit radar mapping for the given model.

The inertial attitude is given with respect to the same coordinate reference frame as the orbit, i.e. J2000, where the axes of the model geometry coincide with the axes of the reference frame when the attitude is represented by the unit quaternion. The given attitude description is in Euler Angles, following the zXZ convention and a positive rotation corresponding with a clockwise rotation when looking along the axis of rotation.

White streaks visible in the radar mappings, which are not generated by shading effects, are an artefact of the radar mapping algorithm when presented with touching facets having different boundary values, at the pixel locations, in the z-buffer. This occurs when two visible and touching facets are close to parallel with the LOS of the observer. The difference in z-buffer coordinates can exceed the resolution of the image, which induces the artificial white-space.

Observation 2012-05-13 11:46:09 details:

- Range: 2482 km, Azimuth: 353° , Elevation: 8° .
- Inertial Attitude: Phi: 163° , Theta: 87° , Psi: 31° .
- Radar mapping inertial axes (unit vectors):
Range: [-0.1719, -0.6608, 0.7305],
Doppler: [0.8214, 0.3131, 0.4766].

Observation 2012-05-13 11:52:18 details:

- Range: 1908 km, Azimuth: 277° , Elevation: 16° .
- Inertial Attitude: Phi: -12° , Theta: 40° , Psi: 168° .
- Radar mapping inertial axes (unit vectors):
Range: [0.9132, -0.2882, 0.2878],
Doppler: [0.3724, 0.3151, -0.8721].

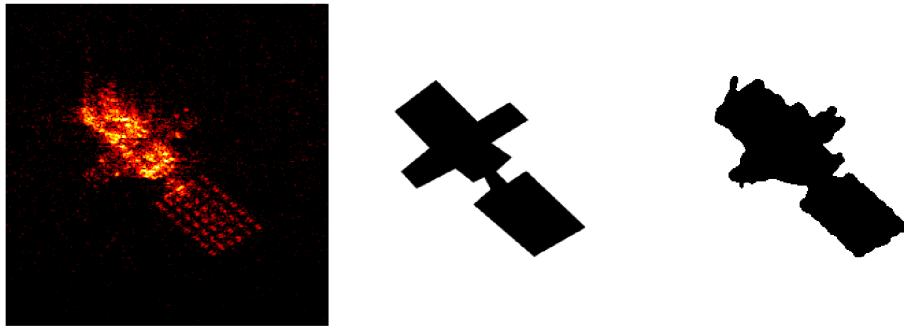


Figure 5: ISAR image by TIRA (Fraunhofer FHR) (left), ISAR image reduction to shape by a human interpreter (middle), ISAR image reduction to shape by a computer algorithm (right), for observation 2012-05-13 11:46:09.

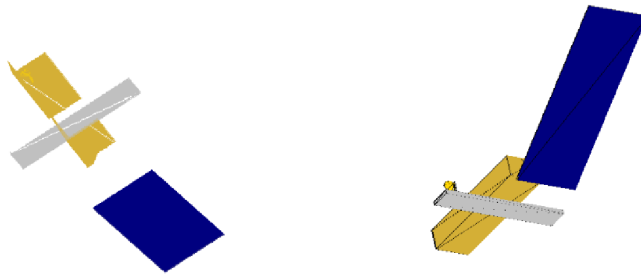


Figure 6: Best fit radar mapping (left) and the corresponding optical observation of the best fit radar mapping (right) for observation 2012-05-13 11:46:09.

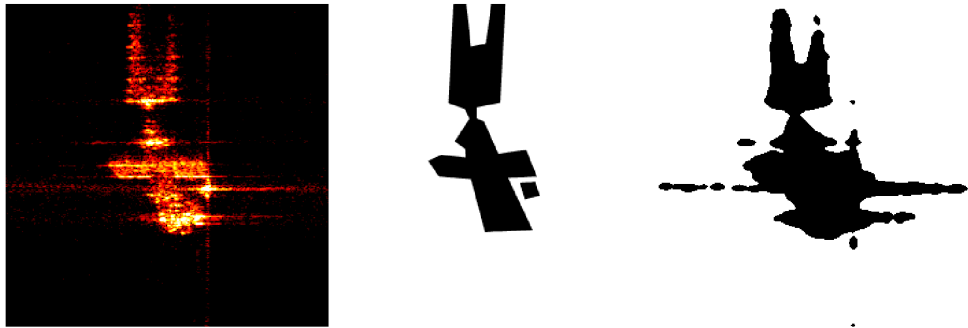


Figure 7: ISAR image by TIRA (Fraunhofer FHR) (left), ISAR image reduction to shape by a human interpreter (middle), ISAR image reduction to shape by a computer algorithm (right), for observation 2012-05-13 11:52:18.

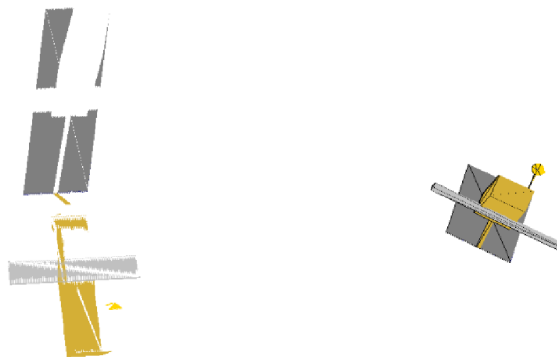


Figure 8: Best fit radar mapping (left) and the corresponding optical observation of the best fit radar mapping (right) for observation 2012-05-13 11:52:18.